

Valley filtering and spatial maps of coupling between silicon donors and quantum dots

J. Salfi,¹ B. Voisin,¹ A. Tankasala,² J. Bocquel,¹ M. Usman,³ M. Y. Simmons,¹ L. C. L. Hollenberg,³ R. Rahman,² and S. Rogge¹

¹*Centre for Quantum Computation and Communication Technology, School of Physics, The University of New South Wales, Sydney, NSW 2052, Australia.*

²*Purdue University, West Lafayette, IN 47906, USA.*

³*Centre for Quantum Computation and Communication Technology, School of Physics, University of Melbourne, Parkville, VIC 3010, Australia.*

(Dated: February 10, 2022)

Exchange coupling is a key ingredient for spin-based quantum technologies since it can be used to entangle spin qubits and create logical spin qubits. However, the influence of the electronic valley degree of freedom in silicon on exchange coupling is presently the subject of important open questions. To experimentally address this question we map the interaction of a single donor coupled to a single-electron quantum dot whose position can be defined with sub-nm precision using a scanning tunneling microscope tip. From the measured map we find that lattice-aperiodic spatial oscillations comprise less than 2 % of exchange, indicating that the donor's $\pm x$ and $\pm y$ valleys are filtered out of these interactions because the quantum dot contains only $\pm z$ valleys. Hence, exchange coupling of a donor and quantum dot is immune to valley-induced variations from in-plane donor positioning errors. Given the electrical tunability of quantum dot wavefunctions, this result is promising to realise uniform quantum dot-mediated interactions of donor qubits.

Following proposals for spin-based quantum computing[1, 2], spin qubits have been demonstrated in, *e.g.*, diamond[3], GaAs[4–7], Si donors and Si quantum dots (QDs)[8–12]. Heisenberg exchange coupling plays a key role in these proposals[1, 2], and exchange coupling has been used experimentally to couple spins over short distances[5, 11] and to define multi-spin qubits[4, 6–10]. The latter can be coupled at longer range via electric interactions[6], as also expected for spin-orbit qubits[13–17]. For highly coherent donor based spin qubits in silicon, super-exchange, exchange and tunneling have been proposed to mediate donor interactions[18], create a fault-tolerant donor surface code[19], and define new qubits[20, 21], respectively, while donor/QD interactions have been probed in recent experiments[21–24].

Due to the central role of tunneling, exchange and superexchange coupling in spin-based quantum computing[1, 2, 4–11, 18–21, 25], the role of valley degrees of freedom of electron wavefunctions in these processes has been the subject of many theoretical studies[26–34]. Notably, atomic-scale disorder in dopant positions[26–32] and QD surface roughness[33, 34] have both been predicted to modulate exchange coupling and two-qubit gate fidelities, due to the lattice-aperiodicity of the valley wavevector, and control schemes to recover two-qubit gate infidelities have been proposed[35, 36]. Yet, the role of valleys in exchange coupling has yet to be probed experimentally, and remains a key open question for electron spin based quantum computing in silicon.

Here, we form a single-electron QD underneath a scanned probe tip, and controllably couple it to a single neutral donor in the silicon lattice using sub-nm control of the position \mathbf{R} of the QD relative to the donor. The energy spectrum and spatial tunneling probability of

the resulting interacting two-electron donor/QD system were measured by single-electron transport[37, 38]. The exchange interaction $J(\mathbf{R})$ between the donor and the QD is found to increase with decreasing R , without any evidence of QD valley phase variation, as expected for an electrostatic QD with $\pm z$ valleys[39] which additionally experiences an atomically flat surface. Notably, oscillations in exchange at lattice-aperiodic spatial frequencies are found to comprise less than 2 % of the nominal donor/QD exchange $J(\mathbf{R})$. This evidences a valley filtering effect discussed in valleytronics literature[40] due to weak inter-valley tunneling and exchange, that has yet to be observed in indirect gap materials. Here, the $\pm x$ and $\pm y$ valleys of the donor, whose wavefunctions contain lattice-aperiodic spatial frequencies, are filtered out of tunneling and exchange because the QD contains only $\pm z$ valleys. The lack of lattice-aperiodic oscillations of donor/QD exchange with in-plane donor position is therefore similar to predictions for donor/donor exchange with enhanced $\pm z$ valley population[28, 29, 41]. These results are promising for the realisation of uniform exchange couplings between highly coherent donors using tunable, electrostatically defined QDs[18–20].

The key ingredient in our experiment is a single-electron QD whose coupling to individual donors can be tuned by controlling the QD position with sub-nm precision, using a scanning tunnelling microscope (STM) tip (Fig. 1a). The QD state is formed below a silicon/vacuum surface when the bands are locally bent downwards by the tip due to a bias V applied to a reservoir (Fig. 1b)[43, 44]. The QD and donor are contained in a lightly doped region, above a highly doped reservoir and below a (100) hydrogen terminated surface (Fig. 1a). The doping gradient was prepared by thermal annealing[37].

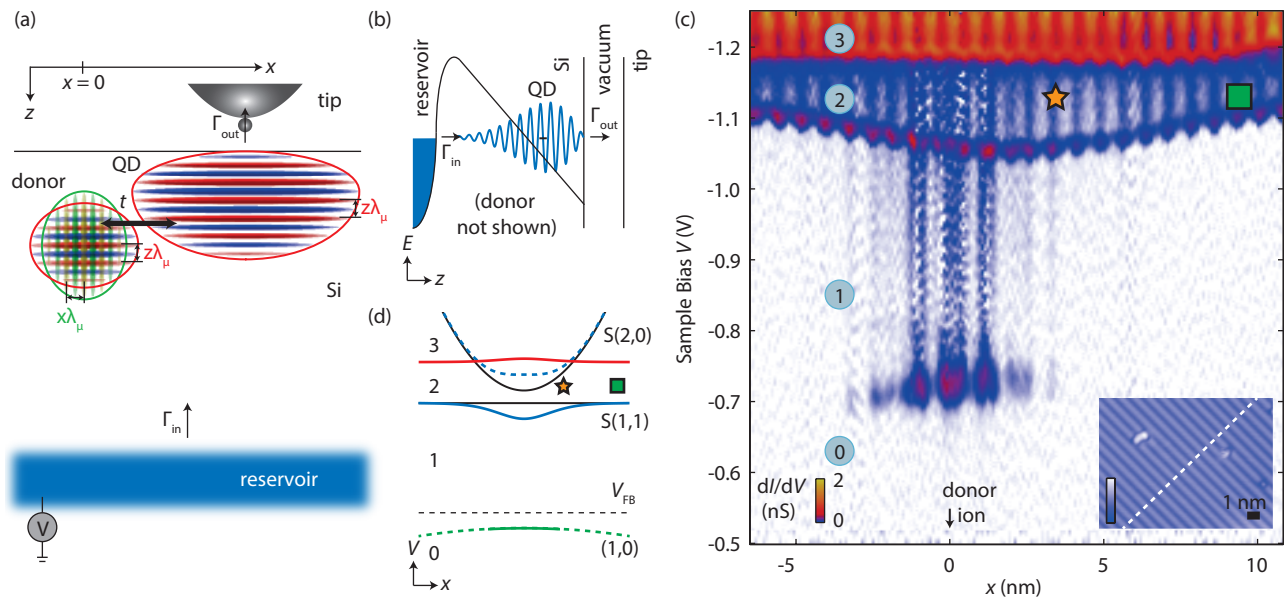


FIG. 1. Schematic of single-electron tunnelling from buried reservoir, to coupled donor/QD state, to the tip. The donor wavefunction parameters are taken from ref. 42, and the $\pm x$ and $\pm z$ valleys participating in the six valley superposition are labelled. $\lambda_\mu = 2\pi/k_\mu$, where $k_\mu = 0.82(2\pi/a_0)$ is the conduction band minimum wavevector, and a_0 is silicon's lattice constant. (b) Schematic diagram of isolated QD resonance created by tip-induced band bending. (c) Measured dI/dV spectrum. Regimes of 0, 1, 2, and 3 electrons are labelled and separated by green, blue, and red lines. The studied donor/QD hybrid resonance separates the 1 and 2 electron regimes. Inset: measured topography, dashed line shows location of dI/dV data. (d) Energy diagram with unhybridized (black lines) and hybridized (blue lines) 2 electron states. Here, $S(i, j)$ is a singlet with i (j) electrons on the donor (QD). Tunnel coupling t hybridizes $S(1,1)$ and $S(2,0)$ forming a ground state (solid blue) and excited state (dashed blue). Temperature: 4.2 K.

The energy of the QD was probed by spatially resolved single-electron tunneling. For the data shown in the dI/dV map of Fig. 1c containing a neutral donor state [37, 45] at $V = -0.80$ V, we identify the first electron in a tip-induced QD state when the bands are bent downward for the resonance at $V \approx -1.10$ V, away from the donor. Notably, the resonance shifts to $V = -1.05$ V as the QD approaches the neutral donor showing that the coupled donor/QD state has a lower energy than the QD, since less downward bias of the localized state (relative to the reservoir) is required for resonant tunneling.

This spatial dependence of the QD resonance in Fig. 1c is inconsistent with a non-interacting state of the donor and QD. Without interactions, the QD energy would be independent of position (Fig. 1d, lower black line), while the observed resonance dips locally around donors. Moreover, charging an isolated donor with a second electron would produce an upward curving $S(2,0)$ resonance (Fig. 1d, upper black line). This is because as the tip moves away from the donor, it is less effective at locally influencing the potential at the donor site [46], so a larger bias is needed to overcome the donor's on-site Coulomb repulsion. In contrast, the resonance in Fig. 1c flattens out, approaching $S(1,1)$ -like behaviour. Consequently the two-electron ($2e$) state in Fig. 1c can only be understood as a hybridized superposition of $S(1,1)$ and

$S(2,0)$ singlets (Fig. 1d, solid blue).

Importantly, the donor/QD system forms a molecular state in Fig. 1c since its exchange energy J well exceeds the reservoir tunnel rates, $h(\Gamma_{\text{in}} + \Gamma_{\text{out}})$. This result is obtained by combining two experimentally established inequalities: First dI/dV has a lineshape of a thermally broadened reservoir (Fig. 2a), so $k_B T > h(\Gamma_{\text{in}} + \Gamma_{\text{out}})$. Second, J well exceeds $k_B T$, as will be shown later.

The $1e$ state identified at $V = -0.80$ V corresponds to the neutral donor's electron tunneling to the tip, and a $1e \rightarrow 0e$ donor charge transition. Resolved in real space at an electric field -1 ± 2 MV/m (Fig. 2b), we identify the A_1 ground state [37, 45], and depth $6.75a_0$ for the donor ($a_0 = 0.543$ nm) using a comprehensive tunnelling image analysis [47]. With the $2e$ donor/QD state in the bias window at $V = -1.125$ V, tunnelling to the tip yields a $2e \rightarrow 1e$ charge transition on the coupled donor/QD that when resolved in real space (Fig. 2c) represents a quasi-particle wavefunction (QPWF) [48–50, 53]. Following $2e \rightarrow 1e$ tunneling, tunneling to the tip ($1e \rightarrow 0e$) is much less likely than tunneling from the reservoir ($1e \rightarrow 2e$) since $\Gamma_{\text{in}} \gg \Gamma_{\text{out}}$ [52]. Consequently, having the donor/QD resonance in the bias window suppresses tunneling from the neutral donor.

For the discussion of the measured QPWF in Fig. 2c we use the spin singlet model from Fig. 1d where $\Psi_S =$

$c_{1,1}\Psi_{S(1,1)} + c_{2,0}\Psi_{S(2,0)}$, $\Psi_{S(i,j)}$ is the singlet with i electrons on the donor and j on the QD, and $c_{i,j}$ is the probability amplitude for $S(i,j)$. The tunneling current is $I(\mathbf{r}) = |\mathbb{D}(2^{-1/2}c_{1,1}\psi_{d_1}(\mathbf{r}))|^2 + |\mathbb{D}(2^{-1/2}c_{1,1}u_q(\mathbf{r}) + c_{2,0}\psi_{d_2}(\mathbf{r}))|^2$, where \mathbb{D} is a differential operator that takes the STM tip orbital into account[47, 54], $\psi_{d_i}(\mathbf{r})$ is the donor orbital for electron number i , and $u_q(\mathbf{r})$ is the lattice-scale part of the QD wavefunction; the QD follows the tip and its full wavefunction cannot be mapped. Indeed, the centre of the donor/QD map (Fig. 2c) is donor-like (Fig. 2b), as expected from the expression for $I(\mathbf{r})$. Moreover, for tip positions where the donor-like signature disappears, the donor/QD resonance (Fig. 2c) is lattice periodic in the (x, y) plane as expected for a QD wavefunction containing only $+z$ and $-z$ Bloch states[55, 56].

Importantly, the QD and donor states have a significant overlap, since the QD charge density is expected to peak at $z_0 \approx 3.5a_0$, just ~ 2 nm from the donor ion at $6.75a_0$. Here, z_0 was estimated using the triangular well approximation[55] with $z_0 \approx 1.32(\hbar^2/2me\mathcal{E}_z)^{1/3}$, where $\mathcal{E}_z = 13 \pm 2$ MV/m is the electric field and m is the

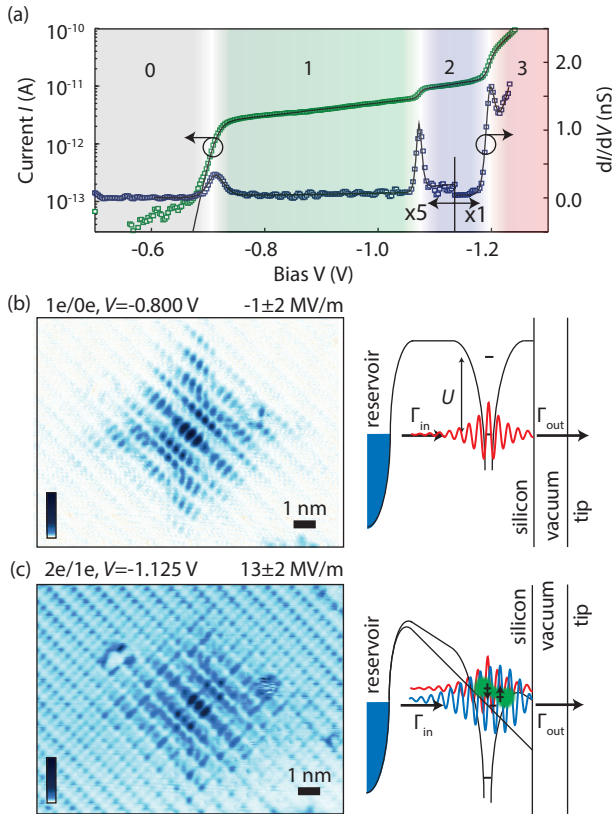


FIG. 2. (a) Bias dependence of current I (green) and conductance dI/dV (blue) over the donor, and fit to rate-equation model (black lines). (b) Measured current map of the neutral donor. Right: tunnel junction energy diagram. (c) Measured current map of coupled donor/QD singlet. Right: tunnel junction energy diagram. Both current maps are for spatial region as the Fig. 1c inset.

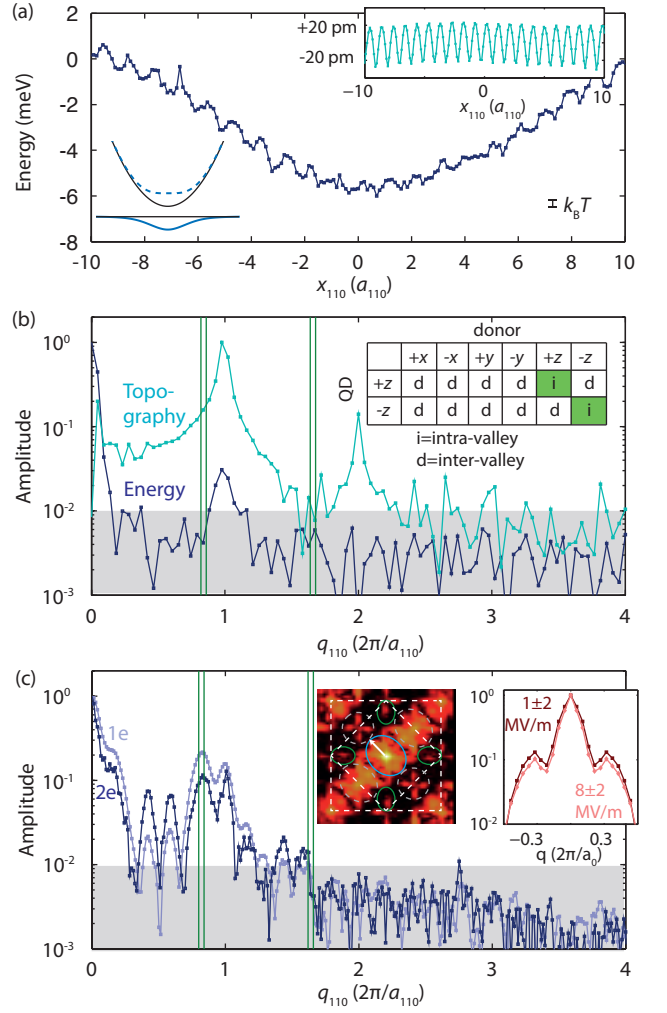


FIG. 3. a. Donor/QD energy $E(x)$ as a function of tip position x . Inset: measured topography. b. Spatial Fourier decomposition of $E(x)$ where lattice-aperiodic components are less than 1% of value at $q_{110} = 0$. Inset: intra-valley (green) and inter-valley (white) tunneling for donor and QD. c. One-dimensional spatial Fourier decomposition of $2e$ and $1e$ tunnelling current along a $[110]$ direction, with lattice aperiodic oscillations due to valley superpositions in donor bound states at $q_{110} = 0.85(2\pi/a_{110})$ and harmonics, where $a_{110} = \sqrt{2}a_0$. Left inset: two-dimensional Fourier decomposition of one-electron tunneling probability at electric field 8 ± 2 MV/m and bias $V = -1.010$ V. Right inset: line cut through two-dimensional decomposition evidencing negligible valley repopulation of donor just below the $2e$ resonance.

longitudinal electron effective mass in Si.

The remainder of the analysis focuses on the dependence of the donor/QD energy $E(x)$ on donor/QD displacement x , which we will show is dominated by the exchange interaction $J(x)$. $E(x)$ in Fig. 3a, obtained from Fig. 1c and the extracted lever arm[52], varies by 5.5 meV over a 16 nm span. Notably, the interface is atomically flat (Fig. 1c, inset), which is important since interface steps and rough Si/SiO₂ surfaces

will influence the valley degree of freedom and exchange coupling of QDs[33, 34, 39, 57–60]. For an atomically flat surface, components to donor/QD exchange coupling involving the donor's x and y valleys yield lattice-aperiodic Fourier components in $E(x)$. This is because the donor/QD energy map $E(x)$ is dominated by exchange coupling $J(x) = J_{dq}(x) + \frac{1}{2}(U_{e1} - \sqrt{8t(x)^2 + U_{e1}^2})$, which in turn contain tunneling and exchange terms $t(x)$ and $J_{dq}(x)$ with lattice-aperiodic components[27]. Here, $U_{e1} = E_d - E_q + U_{dd} - U_{dq}$ is an effective charging energy, U_{dd} is the donor charging energy and U_{dq} is the QD/donor electron repulsion. The remaining contribution to $E(x)$ is the Coulomb interaction of the QD with the neutral donor, estimated to be ~ 1 meV[52]. Importantly, the Fourier decomposition of $E(x)$ (Fig. 3b) contains no lattice-aperiodic components above $\approx 1\%$ of the average of $E(x)$ (at $q_{110} = 0$). Given that $J(x)$ comprises more than 50% of $E(x)$ and the residual Coulomb interactions in $E(x)$ do not have lattice aperiodic components, the 1% upper bound for $E(x)$ corresponds to a 2% upper bound of lattice aperiodic components of $J(x)$.

Tunneling and exchange in a coupled donor/QD system differs from two donors[26, 27, 29–32] because the QD is a superposition of $\pm z$ valleys only, and the donor is a six-valley superposition as evidenced by lattice-aperiodic components in the Fourier transforms of STM tunnel current maps (Fig. 3c). Even at an applied electric field of 8 ± 2 MV/m below the 2e resonance ($V = -1.010$ V), the six-valley donor superposition is weakly perturbed. This is evidenced by the peak at $\mathbf{q} = \pm(+0.15, -0.15)(2\pi/a_0)$ in the right hand inset of Fig. 3c, whose measured amplitude decreases with decreasing x and y valley population[37, 42]. By comparison with theoretical STM images[47], we estimate a 0.5% change in the population of the x and y valleys with the increase in electric field from -1 ± 2 MV/m to 8 ± 2 MV/m[52].

The spectral decomposition of $J(\mathbf{R})$ can be understood within an extended Hubbard model for donor/QD tunneling $t(\mathbf{R}) = \langle \psi_q | v_q + v_d | \psi_d \rangle$ and exchange $J_{dq}(\mathbf{R}) = \langle \psi_d \psi_q | e^2 (4\pi\epsilon |\mathbf{r}_1 - \mathbf{r}_2|)^{-1} | \psi_q \psi_d \rangle$. Here, \mathbf{R} is the donor/QD separation, $v_{d(q)}$ is the donor (QD) potential, $\psi_d(\mathbf{r}) = \sum_{\mu} \psi_{d\mu}(\mathbf{r})$ is a donor wavefunction and $\psi_q(\mathbf{r}) = \sum_{\mu=\pm z} \psi_{q\mu}(\mathbf{r})$ is a QD wavefunction. In $J(\mathbf{R})$, intra-valley (valley preserving) and inter-valley (valley modifying) terms have lattice-aperiodic prefactors $\exp(i\mathbf{k} \cdot \mathbf{R})$, where \mathbf{k} are distributed about the conduction band minima. While the intra-valley tunneling present in donor/donor exchange can be evaluated in the effective mass approximation[27], it is absent here for x and y valleys due to the QD's $\pm z$ valley nature. Only inter-valley tunneling (*e.g.*, x to z valleys in Fig. 1a) contributes lattice-aperiodic terms $\exp(i\mathbf{k} \cdot \mathbf{R})$ to $J(\mathbf{R})$. Although these are expected to be negligible when the spatial extent a of the wavefunctions are much larger than

$a_0 = 0.543$ nm[61], this barely holds in our experiment, since $a \sim 1$ nm for donors, and a is a few nm for our QD with 10 meV charging energy. Theoretical prediction of the inter-valley contributions goes beyond the effective mass approximation, and could be accomplished with more sophisticated techniques[29, 32] that predict J oscillations for two donors, albeit damped[29]. Nevertheless, the weakness of observed lattice-aperiodic exchange indicates that inter-valley exchange terms constitutes less than 2% of the total exchange coupling. Then, the length scale for variations associated with unity scale exchange coupling variations in donor/QD systems is the few nm decay constant of the QD wavefunction, rather than the ~ 1 nm donor Bohr radius and $\pi/k_{\mu} \sim 0.32$ nm valley frequency[27]. Notably, this reasoning applies to tunneling, exchange, and superexchange coupling since each contains terms proportional to t^2 . The uniformity of QD-mediated coupling of donors will further benefit from tuning of the tunnel coupling t to the QD using local gates[19, 20]. This way, similar to donor/donor exchange, residual coupling errors can in principle be corrected by quantum control[35, 36].

A quantitative theory analysis has been carried out to ensure that the measured spatial variation of donor/QD energy is dominated by exchange. The calculations employ a full configuration interaction (FCI) approach with atomistic tight-binding wavefunctions[32, 62]. A 5 nm STM tip radius was chosen to reproduce the bias where $0e \rightarrow 1e$ and $1e \rightarrow 2e$ QD transitions occur, away from the donor. The lowering of the addition energy due to donor/QD coupling when the QD is directly over the donor is calculated to be $E(x=0) = 6.8$ meV, compared to $J(x=0) = 3.8$ meV calculated for the donor/QD singlet/triplet splitting, supporting our claim that $E(x)$ is dominated by $J(x)$.

Finally, we note that $E(x)$ is smooth apart from a 20 cycle lattice periodic oscillation in Fig. 3a. This oscillation is likely an artefact from QD energy and wavefunction changes induced by tip-height variation δz (Fig. 3a, inset). For the former, an energy shift of $\delta E = e\alpha\delta z(\epsilon_{Si}\mathcal{E}_z)$ is expected[38], where $\alpha \approx 0.1$ is the lever arm from our fit. For $\delta z = 40$ pm (Fig. 3a, inset) $\delta E = 0.6$ meV, in agreement with the measured 0.7 meV oscillation. Notably, the smooth exchange variation in Fig. 3a indicates that the valley phase[34, 58, 59] varies little, even though the electric field varies by ~ 3 MV/m due to the change in the resonance voltage from $V = -1.05$ V to $V = -1.10$ V.

In conclusion, we have spatially mapped the energy of a neutral donor coupled to a single-electron QD that can be positioned in the plane with sub-nm accuracy using an STM tip. These capabilities could be used to perform electrical spin readout of donors[63] using STM and for other impurities such as NV centres[64, 65]. We observe a valley filtering effect where x and y valleys in the donor have negligible influence on exchange coupling

with the $\pm z$ -valley QD, evidenced by lattice-aperiodic exchange interaction components constituting less than 2 % of the nominal exchange interaction. Rather, we know that variations in the exchange of the donor/QD system originates from the few nm decay constant of the QD wavefunction. These results highlight that, similar to predictions for donor/donor interactions in strained Si, donor/QD interactions [18–21] do not suffer from valley-induced variations in exchange due to in-plane donor positioning errors. These results are promising for the realisation of uniform exchange couplings between highly coherent donors using tunable, electrostatically defined QDs[18–20] that are compatible with an all donor based approach[1, 66].

The authors would like to thank D. Culcer for helpful discussions. We acknowledge support from the ARC Centre of Excellence for Quantum Computation and Communication Technology (CE110001027), and partial support from the US Army Research Office (W911NF-08-1-0527). JS acknowledges partial support from an ARC DECRA fellowship (DE160101490). The authors acknowledge the use of computational resources from NanoHUB.org/NCN, and the Pawsey Supercomputing Centre with funding from the Australian Government and the Government of Western Australia.

SUPPLEMENTAL MATERIAL

Electric field experienced by donor and QD

In this section we experimentally extract the vertical component \mathcal{E}_z of the tip-induced electric field, which eventually confines a single electron against the vacuum interface of Si in the undoped layer of the sample. It has been modelled using a simple one-dimensional electrostatic description accounting for the dependence of the single-electron tunneling peak voltage U_i on tip height z . In this approach, the electric field in the vacuum is given by $-dU_i/dz$, which is reduced by silicon's relative dielectric constant ϵ_{Si} giving $\mathcal{E}_z = -(\epsilon_{\text{Si}}^{-1})dU_i/dz$ [37, 38]. Electric fields extracted using this procedure are plotted against bias in Fig. 4. Three different peak voltages from Fig. 1c in the main text were tracked: the donor 1e resonance ($i = 1$), the donor/QD 2e resonance ($i = 2$), and the 3e resonance ($i = 3$).

Donor depth and repopulation of valleys due to electric fields in neutral donor state

In this section we perform and theory/experiment comparison showing that the electric field of the tip has a small impact on the valley population one-electron ground state of the donor. As a baseline, we start with wavefunction measurements in the smallest electric field

(Fig. 4, $V = -0.80$ V, $\mathcal{E} = -1 \pm 2$ MV/m), and where single dopants can be pinpointed with lattice precision in three dimensions[47]. We re-plot the Fourier representation of the tunnel current along a [110] direction for \mathbf{q} , for the $6.75a_0$ deep donor discussed throughout the main text ($a_0 = 0.543$ nm) shown in Fig. 5a in the main text. Plotted alongside this data is the same quantity for an applied electric field $\mathcal{E}_z \approx 8 \pm 2$ MV/m at a sample bias $V = -1.010$ V, the same data is shown in Fig. 1c of the main text. Here, the ratio of the side peak at $q \approx 0.22(2\pi/a_0)$ and the main peak at $q = 0$, given in Table I, is proportional to product of x and y valley population[37].

The Fourier decomposition of the predicted STM image for this depth is shown in Fig. 5b, for a uniform electric field $\mathcal{E}_z = 0$ MV/m and 8 MV/m, showing a good agreement with experiment with the tip-induced potential. A detailed analysis of the valley population of the donor, carried out on the tight-binding wavefunction using a basis change with the Slater orbitals described elsewhere[37], reveals only a 1% change in z valley population for the higher field. Based on the good theory/experiment match and the valley repopulation estimate for the theory donor, we estimate the change in z valley population of the measured donor, due to the tip-induced potential that confines the quantum dot (QD), is only around 1 %.

Single-electron tunneling

In the following analysis we show how to extract addition energies for the 1e, 2e, and 3e transitions. We also

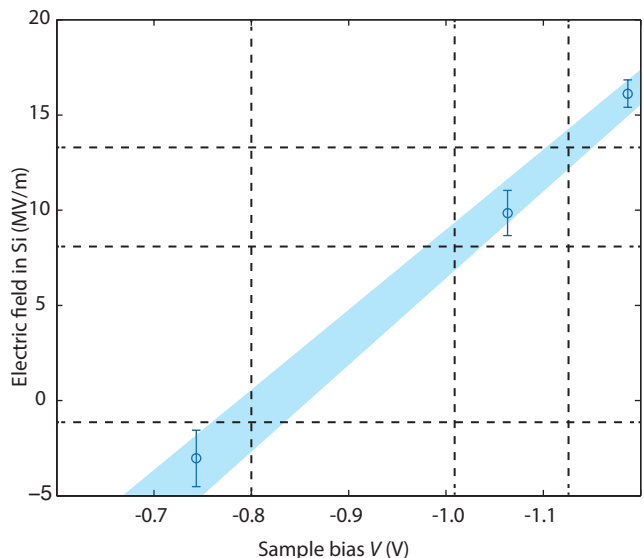


FIG. 4. Bias dependence of electric field extracted from effective one-dimensional model for tip-sample junction.

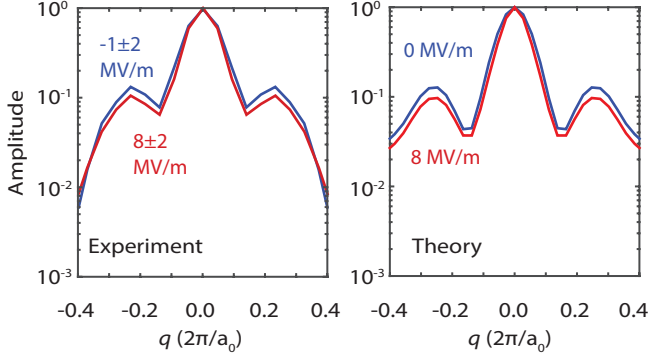


FIG. 5. Profile of donor state Fourier decomposition along [110] direction for (a) measured STM tunnel current and (b) theoretically predicted STM tunnel current, for two different electric fields.

Electric Field	Expmt/Theory	0 MV/m	8 MV/m
Side-lobe ratio	Expmt.	0.13	0.10
Side-lobe ratio	Theory	0.13	0.09
Valley population x, y (%)	Theory	32.8	32.3
Valley population z (%)	Theory	34.5	35.4

TABLE I. Comparison of measured and calculated Fourier spectrum for $z_0 = 6.75a_0$ deep donor in two different electric fields.

show that in the limit $\Gamma_{\text{in}} \ll \Gamma_{\text{out}}$, the presence of the $2 \rightarrow 1$ charge transition in the bias window blocks the $1 \rightarrow 0$ tunneling from contributing to the total current. We employ a classical rate equation analysis of electron tunneling to describe single-electron transport through multiple charge levels in our donor/QD system[67] with thermally broadened reservoirs. The starting point for this model is in ref. 38. Here, this model is generalized to non-zero temperature and multiple charge states. Within this framework, the total current is given by

$$I = \sum_i e\rho_i (\Gamma_{i \rightarrow i-1}^t) \quad (1)$$

Here, ρ_i is the probability of i electron occupation. Moreover, $\Gamma_{i \rightarrow i \pm 1}^t$ is the tunnel rate from (to) the tip causing a charge transition $i \rightarrow i \pm 1$ on the donor/QD system, which is given by the product of a bare tunnel rate $\Gamma_{i, i \pm 1}^t$ and a Fermi-Dirac statistical distribution $f(E_F, E) = (1 + \exp((E - E_F)/k_B T))^{-1}$ for the tip, as follows:

$$\Gamma_{i \rightarrow i-1}^t = \Gamma_{i, i-1}^t [1 - f(eV, E_i - e\alpha_i V)] \quad (2)$$

$$\Gamma_{i-1 \rightarrow i}^t = \Gamma_{i, i-1}^t f(eV, E_i - e\alpha_i V) \quad (3)$$

$$(4)$$

where α_i is the lever-arm for the charge state i with bias V , k_B is Boltzmann's constant, $T = 4.2$ K is the sample temperature, and E_i is the addition energy of the i -

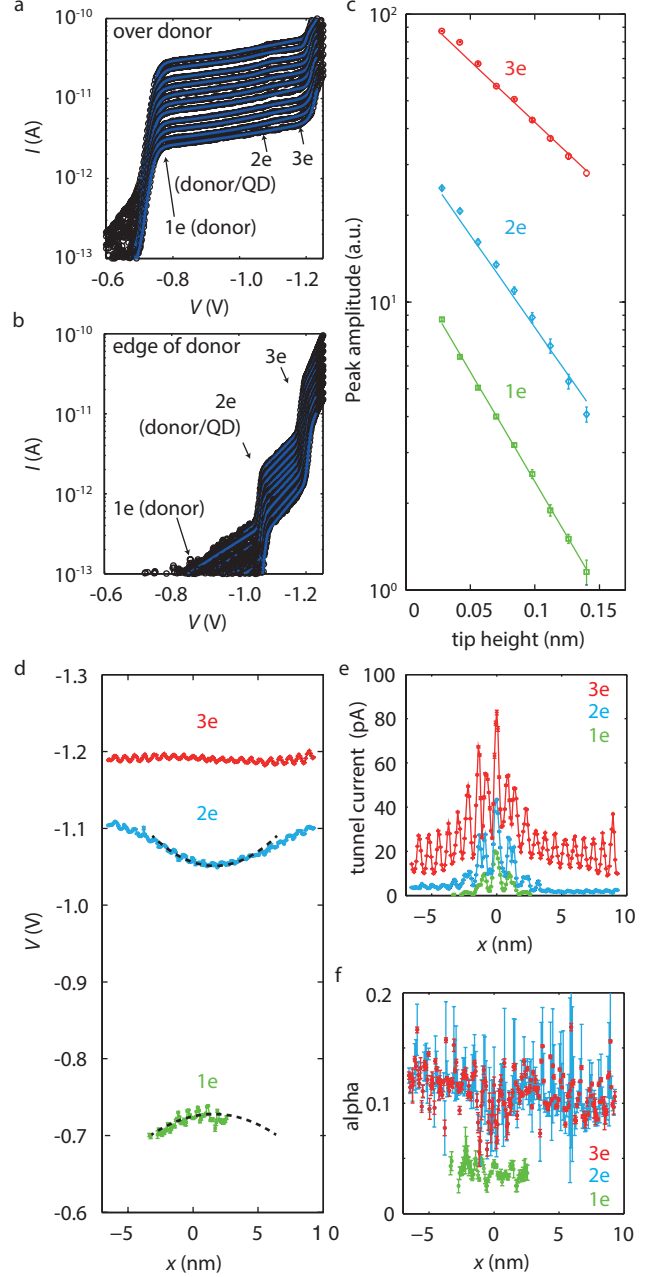


FIG. 6. Current-voltage characteristic of donor/QD system, for a sequence of fixed equally spaced tip heights (a) for tip position at brightest central dimer in donor and (b) for tip position a few nm away from brightest central dimer of donor. c. Dependence of tunnel current amplitude $M_{i, i-1}^{t0}$ step as a function of tip height, and charge number p in the transition $i \rightarrow i - 1$. Spatial fits of single-electron tunneling quantities for the 1e, 2e, and 3e resonances, where $x = 0$ denotes the position of the donor ion. (d) transition voltage V_i , (e) transition current amplitude $e\Gamma_{i, i-1}^{t0}$ (f) tip-sample lever arm α_i . The dashed parabolic lines in (d) show that the 1e and 2e resonances are centred along the same x coordinate, as expected for tip-induced band bending[46].

electron state. Note that in our experiment, the reservoir chemical potential is well below the states being probed, relative to temperature, so that electron tunneling from the tip to the bound state $\Gamma_{i-1 \rightarrow i}^t$ is negligible.

We use a master equation to solve for ρ_i given in ref. 67, which also contains tunneling in and out of the reservoir in the sample, to the quantized states. Noting that the current depends exponentially on tip height, (Fig. 6a,b), we can conclude that $\Gamma_{\text{out}} = \Gamma_{i,i-1}^t$ to the tip is much less than the $\Gamma_{\text{in}} = \Gamma_{i-1,i}^r$ from the reservoir. To zeroth order in $\Gamma_{\text{out}}/\Gamma_{\text{in}}$, our rate equation model yields

$$I = \sum_i \Gamma_{i,i-1}^t f_i (1 - f_{i+1}) \quad (5)$$

where $f_i = (1 + \exp(-e\alpha_i(V - V_i)/k_B T))^{-1}$ is the probability of an electron in the sample reservoir at the energy $E_i = e\alpha V_i$ for the i^{th} charge state.

We fit the measured z -dependent spectrum in Fig. 6a,b. We employ an exponential barrier lowering with bias described by γ_i in $\Gamma_{p,p\pm 1}^t = \Gamma_{p,p\pm 1}^{t_0} \exp(\gamma_i(V - V_i))$. Fits for the tunnel current in the centre of the donor, and a few nm away from the donor, are shown for different tip heights z as blue lines superimposed on the data in Fig. 6a and Fig. 6b, and are in excellent agreement with the data. The extracted values for $\Gamma_{i,i-1}^{t_0}$ as a function of tip height are shown in Fig. 6c, and demonstrate the exponential tip height dependence of current from experiments, as expected. The solution to the rate equations in the limit of small $\Gamma_{i,i-1}^t/\Gamma_{i,i+1}^r$ given in Equation 5 establishes the result that when the $2 \rightarrow 1$ charge transition enters the bias window, the tunnel current reflects only this transition, and blocks the $1 \rightarrow 0$ transition from contributing to the total tunneling current. Finally, the extracted energy for the two-electron state E_i is given in Fig. 3a in the main text.

We fit the x -dependent spectral data in the main text, Fig. 1c to obtain the voltage V_i , lever arm α_i and tunnel rate $\Gamma_{i,i-1}^t$ in this model, and extract the energy $E_i = e\alpha_i V_i$ using V_i and spatially smoothed values of α , as plotted in Fig. 3a. The fit of the peak voltage, current, and lever arms are shown Fig. 6d, e and f. Notably for the peak voltage, close to the donor, the parabolic dependence on tip voltage is centred along the same coordinate $x_o \sim 2$ nm. This offset from the donor center $x = 0$ probably reflects the difference in the location of the centre of mass of the QD wavefunction, and the atom position where tunneling to the tip occurs.

Simplified Hubbard model for spectrum and images

In this section we theoretically discuss a Hubbard model for the energy spectrum and images that is mo-

tivated by features observed in the experiments. Here, the donor-QD system is described by potentials v_d of the donor and v_q of the QD. Defining two single-electron Hamiltonians $h_d = \mathcal{S} + v_d$ and $h_q = \mathcal{S} + v_q$, where \mathcal{S} is the kinetic energy operator, the states of interest in the separated systems corresponding to the donor and QD are ϕ_d and ϕ_q respectively, which satisfy equations $h_d \phi_d = \varepsilon_d \phi_d$ and $h_q \phi_q = \varepsilon_q \phi_q$ respectively. Then in the composite system defined by the total applied potential $v_d + v_q$, the one-electron problem is determined by the Hamiltonian $h = \mathcal{S} + v_d + v_q$, and the two-electron problem is determined by the Hamiltonian $h = h^{(1)} + h^{(2)} + V^{(12)}$ where $h^{(1)} = \mathcal{S}^{(1)} + v_d^{(1)} + v_q^{(1)}$ is a function of coordinate \mathbf{r}_1 only, $h^{(2)} = \mathcal{S}^{(2)} + v_d^{(2)} + v_q^{(2)}$ is a function of coordinate \mathbf{r}_2 only, and $V^{(12)}$ is the electron-electron Coulomb repulsion.

To solve the one and two-electron problems we construct a Wannier basis of maximally localized orbitals[68], $\psi_d = (\phi_d - g\phi_q)/\sqrt{1 + g^2 - 2gS}$ and $\psi_q = (\phi_q - g\phi_d)/\sqrt{1 + g^2 - 2gS}$, where $S = \langle \phi_d | \phi_q \rangle$ is the overlap. The value $g = (1 - \sqrt{1 - S^2})/S$ ensures the orthogonality of the Wannier orbitals, *i.e.*, $\langle d | q \rangle = \langle q | d \rangle = 0$, while the normalization $\langle d | d \rangle = \langle q | q \rangle = 1$ is ensured by the prefactor $1/\sqrt{1 + g^2 - 2gS}$.

One-electron spectrum

For the one-electron Hamiltonian in the Wannier basis $\{\psi_d(\mathbf{r}), \psi_q(\mathbf{r} - \mathbf{R})\}$, the eigenstates obey

$$\left(\left(\frac{E_d + E_q}{2} \right) \mathbb{I} + \begin{pmatrix} -\frac{\Delta}{2} & t(\mathbf{R}) \\ t(\mathbf{R}) & \frac{\Delta}{2} \end{pmatrix} \right) \Psi = E \Psi \quad (6)$$

where \mathbb{I} is the identity matrix, $\Delta = E_q - E_d$ is the donor/QD detuning, $t = \langle d | h | q \rangle$ is the tunneling from ψ_d to ψ_q due to the total potential of the donor and tip, and energies $E_d = \langle d | h | d \rangle = \varepsilon_d + \langle d | v_q | d \rangle$ and $E_q = \langle q | h | q \rangle = \varepsilon_q + \langle q | v_d | q \rangle$ reflect confinement by v_d and v_q due to the donor and tip. The eigenenergies are:

$$E_{\pm} = \frac{E_d + E_q}{2} \pm \frac{1}{2} \sqrt{\Delta^2 + 4t^2} \quad (7)$$

Two-electron spectrum

We expand the two-electron problem in a basis of singlets and triplets of the QD and donor Wannier functions written above. The singlets Ψ_S and triplets Ψ_T are

$$\Psi_{S(1,1)}(\mathbf{r}_1, \mathbf{r}_2) = \frac{1}{\sqrt{2}} (\psi_d(\mathbf{r}_1)\psi_q(\mathbf{r}_2 - \mathbf{R}) + \psi_q(\mathbf{r}_1 - \mathbf{R})\psi_d(\mathbf{r}_2)) |S\rangle \quad (8)$$

$$\Psi_{S(2,0)}(\mathbf{r}_1, \mathbf{r}_2) = \psi_d(\mathbf{r}_1)\psi_d(\mathbf{r}_2) |S\rangle \quad (9)$$

$$\Psi_{S(0,2)}(\mathbf{r}_1, \mathbf{r}_2) = \psi_q(\mathbf{r}_1 - \mathbf{R})\psi_q(\mathbf{r}_2 - \mathbf{R}) |S\rangle \quad (10)$$

$$\Psi_{T^0}(\mathbf{r}_1, \mathbf{r}_2) = \frac{1}{\sqrt{2}} (\psi_d(\mathbf{r}_1)\psi_q(\mathbf{r}_2 - \mathbf{R}) - \psi_q(\mathbf{r}_1 - \mathbf{R})\psi_d(\mathbf{r}_2)) |T^0\rangle \quad (11)$$

$$\Psi_{T^-}(\mathbf{r}_1, \mathbf{r}_2) = \frac{1}{\sqrt{2}} (\psi_d(\mathbf{r}_1)\psi_q(\mathbf{r}_2 - \mathbf{R}) - \psi_q(\mathbf{r}_1 - \mathbf{R})\psi_d(\mathbf{r}_2)) |T^-\rangle \quad (12)$$

$$\Psi_{T^+}(\mathbf{r}_1, \mathbf{r}_2) = \frac{1}{\sqrt{2}} (\psi_d(\mathbf{r}_1)\psi_q(\mathbf{r}_2 - \mathbf{R}) - \psi_q(\mathbf{r}_1 - \mathbf{R})\psi_d(\mathbf{r}_2)) |T^+\rangle \quad (13)$$

where $|S\rangle = \frac{1}{\sqrt{2}} (|\uparrow\downarrow\rangle - |\downarrow\uparrow\rangle)$, $|T^0\rangle = \frac{1}{\sqrt{2}} (|\uparrow\downarrow\rangle + |\downarrow\uparrow\rangle)$, $|T^+\rangle = |\uparrow\uparrow\rangle$, and $|T^-\rangle = |\downarrow\downarrow\rangle$.

We evaluate all the matrix elements of $h = h^{(1)} +$

$h^{(2)} + V^{(12)}$ in the above basis. The singlet and triplet subspaces separate due to their spin orthogonality. The singlet subspace is described by

$$\left((E_d + E_q + U_{dq} + J_{dq}(\mathbf{R}))\mathbb{I} + \begin{pmatrix} 0 & \sqrt{2}t(\mathbf{R}) & \sqrt{2}t(\mathbf{R}) \\ \sqrt{2}t(\mathbf{R}) & U_{e1} & 0 \\ \sqrt{2}t(\mathbf{R}) & 0 & U_{e2} \end{pmatrix} \right) \Psi = E\Psi \quad (14)$$

where $U_{e1} = (E_d + U_{dd}) - (E_q + U_{dq} + J_{dq}(\mathbf{R}))$ is an effective charging energy to put two electrons on the donor, $U_{e2} = (E_q + U_{qq}) - (E_d + U_{dq} + J_{dq}(\mathbf{R}))$ is an effective charging energy to put two electrons on the QD, $U_{qq} = \langle dd|V_{12}|dd\rangle$ is the charging energy of the donor level, $U_{dq} = \langle dq|V_{12}|dq\rangle$ is the mutual Coulomb repulsion of the QD and donor, $U_{qq} = \langle qq|V_{12}|qq\rangle$ is the charging energy of the QD level, and $J_{dq} = \langle qd|V_{12}|dq\rangle$ is an exchange interaction. The simplest limit is to diagonalize the upper 2×2 block assuming that double occupation of the QD is unlikely ($U_{e2} - U_{e1} \gg t$), giving

$$E_S = E_d + E_q + U_{dq} + J_{dq} + \frac{1}{2} \left(U_{e1} - \sqrt{8t^2 + U_{e1}^2} \right), \quad (15)$$

while the triplet energy is given straightforwardly by $E_T = E_d + E_q + U_{dq} - J_{dq}$.

Two cases, $U_{e1} > 0$ (Fig. 7a, blue lines) and $U_{e1} < 0$ (Fig. 7b, blue lines) give qualitatively similar results for E_S . For reference, we show the results ignoring tunnel couplings (black lines, Fig. 7a,b).

Donor/QD resonance transition energy

When the single-electron donor/QD detuning Δ is much larger than the two-electron effective charging energy, as expected for our experiments, we obtain a transition energy

$$E_S - E_1 = E_q + U_{dq} + J_{dq} + \frac{1}{2} \left(U_{e1} - \sqrt{8t^2 + U_{e1}^2} \right). \quad (16)$$

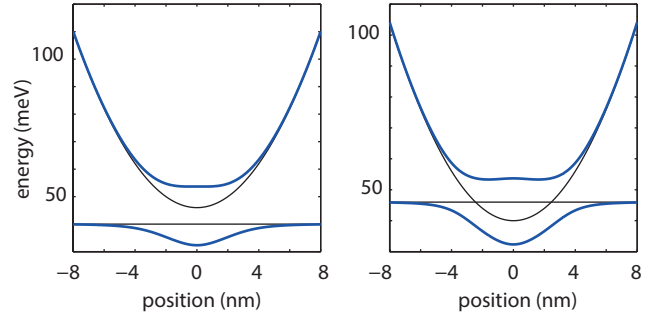


FIG. 7. A. Case where $U_{e1} > 0$ (black lines) and with tunnel coupling turned on (blue lines). B. Case where $U_{e1} < 0$ (black lines) and with tunnel coupling turned on (blue lines).

From the definitions of E_q and U_{dq} we obtain

$$E_q + U_{dq} = \varepsilon_q + \langle q|v_d|q\rangle + U_{dq}, \quad (17)$$

where ε_q is the energy of the non-interacting QD's ground state, and the final two terms $E_{q,D^0} = \langle q|v_d|q\rangle + U_{dq}$ are the Coulombic interaction of the QD with the neutral donor. Finally we rewrite the transition energy as

$$E_S - E_1 = \varepsilon_q + E_{q,D^0} + J_{dq} + \frac{1}{2} \left(U_{e1} - \sqrt{8t^2 + U_{e1}^2} \right). \quad (18)$$

The purely Coulombic interaction E_{q,D^0} of the neutral donor and the QD was calculated using

$$E_{q,D^0} = \langle q|v_d|q \rangle + U_{dq} = \int d\mathbf{r}_2^3 |\psi_q(\mathbf{r}_2 - \mathbf{R})|^2 \frac{-e^2}{4\pi\epsilon_0\epsilon_{Si}r_2} + \int d\mathbf{r}_1^3 d\mathbf{r}_2^3 |\psi_q(\mathbf{r}_2 - \mathbf{R})|^2 \frac{e^2}{4\pi\epsilon_0\epsilon_{Si}|\mathbf{r}_1 - \mathbf{r}_2|} |\psi_d(\mathbf{r}_1)|^2 \quad (19)$$

where we have assumed the donor is at the origin. Evaluating this integral using a Monte Carlo technique we find that E_{q,D^0} varies in space and peaks at ~ 1 meV for $\mathbf{R} = 0$ when the QD overlaps the donor strongest. The small value of this interaction is attributed to the fact that the donor is neutral. Then, the transition energy should be dominated by exchange terms

$$J(\mathbf{R}) = J_{dq}(\mathbf{R}) + \frac{1}{2} \left(U_{e1} - \sqrt{8t(\mathbf{R})^2 + U_{e1}^2} \right) \quad (20)$$

accounting for most of the 5.5 meV spatial variation in energy $E(x)$ for Fig. 3a in the main text.

2 \rightarrow 1 transition image

The donor/QD system forms a molecule weakly probed by single-electron tunneling by the reservoirs[49], such that the STM image represents a quasi-particle wavefunction[48]. For our two-electron state $\Psi_S(\mathbf{r}_1, \mathbf{r}_2) = c_{11}\Psi_{S(1,1)}(\mathbf{r}_1, \mathbf{r}_2) + c_{20}\Psi_{S(2,0)}(\mathbf{r}_1, \mathbf{r}_2)$ and 2 \rightarrow 1 transition, the quasiparticle wavefunction is

$$\Psi_Q^{2 \rightarrow 1i}(\mathbf{r}) = \int d\mathbf{r}' \Psi_S^*(\mathbf{r}', \mathbf{r}) \psi_i(\mathbf{r}') \quad (21)$$

for a single-electron final state $\psi_i(\mathbf{r})$. Then the total current is the sum of currents for each possible final state, given by $I(\mathbf{r}) = \sum_i |\mathbb{D}(\Psi_Q^{2 \rightarrow 1i}(\mathbf{r}))|^2$, where \mathbb{D} is a derivative operator accounting for the orbital content of the STM tip[54]. The tip orbital with d-like symmetry $d_{z^2-1/3r^2}$ has been found to be important to describe real space STM images of donor-bound electrons in silicon[47]. Considering two possible final states, the one-electron donor state and the one-electron QD state, we obtain

$$I(\mathbf{r}) = |\mathbb{D}(c_{11}2^{-1/2}\psi_q(\mathbf{r}) + c_{20}\psi_{d_2}(\mathbf{r}))|^2 + |\mathbb{D}(c_{11}2^{-1/2}\psi_{d_1}(\mathbf{r}))|^2. \quad (22)$$

Since the QD follows the tip, we note that only the lattice-periodic component of the QD wavefunction $u_q(\mathbf{r})$ can be detected, so we must replace $\psi_q(\mathbf{r})$ with $u_q(\mathbf{r})$. Doing this we obtain the expression for $I(\mathbf{r})$ presented in the main text.

Full configuration interaction model

A full configuration interaction approach using tight-binding wavefunctions, used in ref. 62 to model two-electron states of donors in uniform electric fields, was

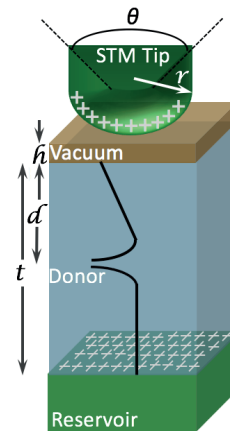


FIG. 8. Schematic of parameters used to describe the electrostatics of the tip and sample. Here, θ = the opening angle of tip, r = tip radius, h = tip height above silicon/vacuum interface. Two additional parameters d describe the donor depth and t the sample reservoir depth below the silicon/vacuum interface.

used to model the interactions of the donor and tip-induced QD. Here, the uniform electric field is replaced by a non-uniform potential of an STM tip, as necessary for the STM tip to induce a QD as observed. We describe a procedure for calibrating parameters for the tip-induced potential shown schematically in Fig. 8, and give some details on how the results quoted in the main text are obtained. Note that the depth d is fixed by single-donor metrology, for measurements taken near the flat-band condition[47].

First, we performed electrostatic calculations of the STM/vacuum/silicon junction using finite element analysis. Then we obtain the single electron energies and wavefunctions of the dot or hybrid donor-dot using atomistic the tight-binding technique including the electrostatic potential. The simulations were done in NEMO3D[69]. Then using the single electron wavefunctions, a basis of two-electron Slater Determinants is constructed and full configuration interaction calculations are performed taking into account the image charges, as described in ref. 62. Diagonalizing the FCI Hamiltonian, the computed 2e total energies, charging energies and singlet-triplet splittings were obtained.

The STM tip parameters were fixed by comparing the binding energy and charging energy of the QD state when it is far away from the donor, at the boundaries of Fig. 1c in the main text. In our experiment, relative to the flat-band voltage ($V \approx -0.8$ V, Fig. 4), a sample bias $\delta V = -0.3$ V (actual bias $V = -1.1$ V) and $\delta V = -0.4$

V (actual bias $V = -1.2$ V) are required to bring the state into resonance with the sample reservoir. We could reproduce these binding and charging transitions using a tip radius of $r = 5$ nm, for an expected reservoir depth of $t = 15$ nm, a tip opening angle assumed to be $\theta = 45^\circ$ and tip height $h = 0.15$ nm. Variations in the tip opening angle and tip height were found to have less of an influence than the tip radius and reservoir depth. Reproducing the binding and charging transition voltages gives us confidence that the Bohr radius of the tip-induced QD is similar to the actual value in experiments.

For these tip and reservoir parameters, we estimated the modulation of the two-electron energy when the single-electron QD interacts with the single electron of the neutral donor at the depth determined from our experiments. In our transport experiment this is equivalent to comparing the $0e \rightarrow 1e$ transition energy of the QD state in the absence of interactions with the donor (the QD binding energy), to the $1e \rightarrow 2e$ transition energy of the QD/donor state, when the tip-induced dot is directly above the donor.

For a donor at $6.75a_0$ we obtain $\Delta E = 53.3$ meV - 46.5 meV = 6.8 meV, which is very similar to the value 5.5 meV from experiments. Assuming a donor one unit cell closer to the surface at $5.75a_0$ gives $\Delta E = 56.7$ meV - 46.5 meV = 10.2 meV, a larger interaction. This is because a donor closer to the surface has a larger overlap, and therefore exchange interaction, with the QD.

-
- [1] B. E. Kane, *Nature* **393**, 133 (1998).
- [2] D. Loss and D. P. DiVincenzo, *Phys. Rev. A* **57**, 120 (1998).
- [3] L. Childress, M. V. G. Dutt, T. J. M. A. S. Zibrov, F. Jelezko, J. Wrachtrup, P. R. Hemmer, and M. D. Lukin, *Science* **314**, 281 (2006).
- [4] J. R. Petta, A. C. Johnson, J. M. Taylor, E. A. Laird, A. Yacoby, M. D. Lukin, C. M. Marcus, M. P. Hanson, and A. C. Gossard, *Science* **309**, 2180 (2005).
- [5] K. C. Nowack, M. Shafiei, M. Laforest, G. E. D. K. Prawiroatmodjo, L. R. Schreiber, C. Reichl, W. Wegscheider, and L. M. K. Vandersypen, *Science* **333**, 1269 (2011).
- [6] M. D. Shulman, O. E. Dial, S. P. Harvey, H. Bluhm, V. Umansky, and A. Yacoby, *Science* **336**, 202 (2012).
- [7] J. Medford, J. Beil, T. J. M. A. S. D. Bartlett, A. C. Doherty, E. I. Rashba, D. P. DiVincenzo, H. Lu, A. C. Gossard, and C. M. Marcus, *Nature Nanotech* **8**, 654 (2013).
- [8] B. M. Maune, M. G. Borselli, B. Huang, T. D. Ladd, P. W. Deelman, K. S. Holabird, A. A. Kiselev, I. Alvarado-Rodriguez, R. S. Ross, A. E. Schmitz, M. Sokolich, C. A. Watson, M. F. Gyure, and A. T. Hunter, *Nature* **481**, 344 (2012).
- [9] D. Kim, Z. Shi, C. B. Simmons, D. R. Ward, J. R. Prance, T. S. Koh, J. K. Gamble, D. E. Savage, M. G. Lagally, M. Friesen, S. N. Coppersmith, and M. A. Eriksson, *Nature* **511**, 70 (2014).
- [10] M. D. Reed, B. M. Maune, R. W. Andrews, M. G. Borselli, K. Eng, M. P. Jura, A. A. Kiselev, T. D. Ladd, S. T. Merkel, I. Milosavljevic, E. J. Pritchett, M. T. Rakher, R. S. Ross, A. E. Schmitz, A. Smith, J. A. Wright, M. F. Gyure, and A. T. Hunter, *Phys. Rev. Lett.* **116**, 110402 (2016).
- [11] M. Veldhorst, C. H. Yang, J. C. C. Hwang, W. Huang, J. P. Dehollain, J. T. Muhonen, S. Simmons, A. Laucht, F. E. Hudson, K. M. Itoh, A. Morello, and A. S. Dzurak, *Nature* **526**, 410 (2015).
- [12] J. J. Pla, K. Y. Tan, J. P. Dehollain, W. H. Lim, J. J. L. Morton, D. N. Jamieson, A. S. Dzurak, and A. Morello, *Nature* **489**, 541 (2012).
- [13] C. Flindt, A. S. Sørensen, and K. Flensberg, *Phys. Rev. Lett.* **97**, 240501 (2006).
- [14] K. C. Nowack, F. H. L. Koppens, Y. V. Nazarov, and L. M. K. Vandersypen, *Science* **318**, 1430 (2007).
- [15] S. Nadj-Perge, S. M. Frolov, E. P. A. M. Bakkers, and L. P. Kouwenhoven, *Nature* **468**, 1084 (2010).
- [16] J. Salfi, J. A. Mol, D. Culcer, and S. Rogge, *Phys. Rev. Lett.* **116**, 246801 (2016).
- [17] J. Salfi, M. Tong, S. Rogge, and D. Culcer, *Nanotechnology* **27**, 244001 (2016).
- [18] V. Srinivasa, H. Xu, and J. M. Taylor, *Phys. Rev. Lett.* **114**, 226803 (2015).
- [19] G. Pica, B. W. Lovett, R. N. Bhatt, T. Schenkel, and S. A. Lyon, *Phys. Rev. B* **93**, 035306 (2016).
- [20] G. Tosi, F. A. Mohiyaddin, S. B. Tenberg, R. Rahman, G. Klimeck, and A. Morello, *arXiv* (2015), 1509.08538.
- [21] P. Harvey-Collard, N. T. Jacobson, M. Rudolph, J. Dominguez, G. A. T. Eyck, J. R. Wendt, T. Pluym, J. K. Gamble, M. P. Lilly, M. Piore-Ladrière, and M. S. Carroll, *arXiv* (2015), 1512.01606.
- [22] G. P. Lansbergen, R. Rahman, C. J. Wellard, I. Woo, J. Caro, N. Collaert, S. Biesemans, G. Klimeck, L. C. L. Hollenberg, and S. Rogge, *Nature Physics* **4**, 656 (2008).
- [23] R. H. Foote, D. R. Ward, J. R. Prance, J. K. Gamble, E. Nielsen, B. Thorgrimsson, D. E. Savage, A. L. Saraiva, M. Friesen, S. N. Coppersmith, and M. A. Eriksson, *Appl. Phys. Lett.* **107**, 103112 (2015).
- [24] M. Urdampilleta, A. Chatterjee, C. C. Lo, T. Kobayashi, J. Mansir, S. Barraud, A. C. Betz, S. Rogge, M. F. Gonzalez-Zalba, and J. J. L. Morton, *Phys. Rev. X* **5**, 031024 (2015).
- [25] M. J. Rančić and G. Burkard, (2017), 1705.03702.
- [26] P. R. Cullis and J. R. Marko, *Phys. Rev. B* **1**, 632 (1970).
- [27] B. Koiller, X. Hu, and S. Das Sarma, *Phys. Rev. Lett.* **88**, 027903 (2001).
- [28] B. Koiller, X. Hu, and S. Das Sarma, *Phys. Rev. B* **66**, 115201 (2002).
- [29] C. Wellard and L. Hollenberg, *Phys. Rev. B* **72**, 085202 (2005).
- [30] G. Pica, B. W. Lovett, R. N. Bhatt, and S. A. Lyon, *Phys. Rev. B* **89**, 235306 (2014).
- [31] J. K. Gamble, N. T. Jacobson, E. Nielsen, A. D. Baczewski, J. E. Moussa, I. Montañó, and R. P. Muller, *Phys. Rev. B* **91**, 235318 (2015).
- [32] Y. Wang, A. Tankasala, L. C. L. Hollenberg, G. Klimeck, M. Y. Simmons, and R. Rahman, *npj Quantum Inf.* **2**, 16008 (2016).
- [33] E. Nielsen, R. Rahman, and R. P. Muller, *Journal of Applied Physics* **112**, 114304 (2012).
- [34] N. Zimmerman, P. Huang, and D. Culcer, *arXiv* (2016),

- 1608.06881.
- [35] M. J. Testolin, C. D. Hill, C. J. Wellard, and L. C. L. Hollenberg, *Phys. Rev. A* **76**, 012302 (2007).
- [36] C. D. Hill, *Phys. Rev. Lett.* **98**, 180501 (2007).
- [37] J. Salfi, J. A. Mol, R. Rahman, G. Klimeck, M. Y. Simmons, L. C. L. Hollenberg, and S. Rogge, *Nature Materials* **13**, 605 (2014).
- [38] B. Voisin, J. Salfi, J. Bocquel, R. Rahman, and S. Rogge, *J. Phys.: Condens. Matter* **27**, 154203 (2015).
- [39] C. H. Yang, A. Rossi, R. Ruskov, N. S. Lai, F. A. Mohiyaddin, S. Lee, C. Tahan, G. Klimeck, A. Morello, and A. S. Dzurak, *Nat Comms* **4**, 1 (2013).
- [40] A. Rycerz, J. Tworzydło, and C. W. J. Beenakker, *Nature Physics* **3**, 172 (2007).
- [41] J. Verduijn, G. C. Tettamanzi, and S. Rogge, *Nano Lett.* **13**, 1476 (2013).
- [42] A. L. Saraiva, J. Salfi, J. Bocquel, B. Voisin, S. Rogge, R. B. Capaz, M. J. Calderón, and B. Koiller, *Phys. Rev. B* **93**, 045303 (2016).
- [43] M. Morgenstern, V. Gudmundsson, R. Dombrowski, C. Wittneven, and R. Wiesendanger, *Phys. Rev. B* **63**, 201301 (2001).
- [44] N. M. Freitag, L. A. Chizhova, P. Nemes-Incze, C. R. Woods, R. V. Gorbachev, Y. Cao, A. K. Geim, K. S. Novoselov, J. Burgdörfer, F. Libisch, and M. Morgenstern, *Nano Lett.* **16**, 5798 (2016).
- [45] K. Sinthiptharakoon, S. R. Schofield, P. Studer, V. Brázdová, C. F. Hirjibehedin, D. R. Bowler, and N. J. Curson, *J. Phys.: Condens. Matter* **26**, 012001 (2014).
- [46] K. Teichmann, M. Wenderoth, S. Loth, R. Ulbrich, J. Garleff, A. Wijnheijmer, and P. Koenraad, *Phys. Rev. Lett.* **101**, 076103 (2008).
- [47] M. Usman, J. Bocquel, J. Salfi, B. Voisin, A. Tankasala, R. Rahman, M. Y. Simmons, S. Rogge, and L. C. L. Hollenberg, *Nature Nanotech* **11**, 763 (2016).
- [48] M. Rontani and E. Molinari, *Phys. Rev. B* **71**, 233106 (2005).
- [49] J. Salfi, J. A. Mol, R. Rahman, G. Klimeck, M. Y. Simmons, L. C. L. Hollenberg, and S. Rogge, *Nat Comms* **7**, 11342 (2016).
- [50] G. Maruccio, M. Janson, A. Schramm, C. Meyer, T. Matsui, C. Heyn, W. Hansen, R. Wiesendanger, M. Rontani, and E. Molinari, *Nano Lett.* **7**, 2701 (2007).
- [51] Supplemental Material.
- [52] F. Schulz, M. Ijäs, R. Drost, S. K. Hämäläinen, A. Harju, A. P. Seitsonen, and P. Liljeroth, *Nature Physics* (2015).
- [53] C. J. Chen, *Phys. Rev. B* **42**, 8841 (1990).
- [54] T. Ando, *Rev. Mod. Phys.* **54**, 437 (1982).
- [55] T. B. Boykin, G. Klimeck, M. Friesen, S. N. Copper-smith, P. von Allmen, F. Oyafuso, and S. Lee, *Phys. Rev. B* **70**, 165325 (2004).
- [56] S. Goswami, K. A. Slinker, M. Friesen, L. M. McGuire, J. L. Truitt, C. Tahan, L. J. Klein, J. O. Chu, P. M. Mooney, D. W. van der Weide, R. Joynt, S. N. Copper-smith, and M. A. Eriksson, *Nature Physics* **3**, 41 (2006).
- [57] P. Boross, G. Széchenyi, D. Culcer, and A. Pályi, *Phys. Rev. B* **94**, 035438 (2016).
- [58] R. Ferdous, E. Kawakami, P. Scarlino, M. P. Nowak, D. R. Ward, D. E. Savage, M. G. Lagally, S. N. Copper-smith, M. Friesen, M. A. Eriksson, L. M. K. Vandersypen, and R. Rahman, *arXiv* (2017), 1702.06210.
- [59] W. Huang, M. Veldhorst, N. M. Zimmerman, A. S. Dzurak, and D. Culcer, *Phys. Rev. B* **95**, 075403 (2017).
- [60] J. Luttinger and W. Kohn, *Phys. Rev.* **97**, 869 (1955).
- [61] A. Tankasala, J. Salfi, J. Bocquel, B. Voisin, M. Usman, G. Klimeck, M. Y. Simmons, L. C. L. Hollenberg, S. Rogge, and R. Rahman, *arXiv* (2017), 1703.04175.
- [62] A. Morello, J. J. Pla, F. A. Zwanenburg, K. W. Chan, K. Y. Tan, H. Huebl, M. Möttönen, C. D. Nugroho, C. Yang, J. A. van Donkelaar, A. D. C. Alves, D. N. Jamieson, C. C. Escott, L. C. L. Hollenberg, R. G. Clark, and A. S. Dzurak, *Nature* **467**, 687 (2010).
- [63] A. Brenneis, L. Gaudreau, M. Seifert, H. Karl, M. S. Brandt, H. Huebl, J. A. Garrido, F. H. L. Koppens, and A. W. Holleitner, *Nature Nanotech* **10**, 135 (2015).
- [64] E. Bourgeois, A. Jarmola, P. Siyushev, M. Gulka, J. Hruby, F. Jelezko, D. Budker, and M. Nesladek, *Nat Comms* **6**, 8577 (2015).
- [65] C. D. Hill, E. Peretz, S. J. Hile, M. G. House, M. Fuechsle, S. Rogge, M. Y. Simmons, and L. C. L. Hollenberg, *Science Advances* **1**, e1500707 (2015).
- [66] E. Bonet, M. M. Deshmukh, and D. C. Ralph, *Phys. Rev. B* **65**, 045317 (2002).
- [67] J. Schliemann, D. Loss, and A. MacDonald, *Phys. Rev. B* **63**, 085311 (2001).
- [68] R. Rahman, S. Park, J. Cole, A. Greentree, R. Muller, G. Klimeck, and L. Hollenberg, *Phys. Rev. B* **80**, 035302 (2009).